JOURNAL OF APPLIED ELECTROCHEMISTRY **27** (1997) 135–145

# Lactic acid production by electrodialysis Part II: Modelling

N. BONIARDI, R. ROTA*, G. NANO, B. MAZZA

*Dipartimento di Chimica Fisica Applicata, Politecnico di Milano, via Mancinelli 7, 20131 Milano, Italy*

Received 25 September 1995; revised 19 June 1996

One interesting alternative to the usual end-of-pipe processes for treating waste water produced during cheese-making involves its fermentation to sodium lactate. Then, electrodialysis can be used to recover free lactic acid from the fermentation broth. The design and optimization of such a process is aided by a suitable mathematical model. This work presents a model of the performance of an electrodialysis stack to be used in such a process. Its reliability has been assessed by comparison with experimental data for free lactic acid recovery from sodium lactate solutions. A suitable procedure for estimating some process-dependent parameters is also discussed.

**List of symbols**

| | |
|---|---|
| $A$ | surface area of each membrane ($m^2$) |
| $a$ | compartment thickness (m) |
| $B$ | constant, $F\,D\,/\,\Lambda$ |
| $C$ | concentration (mol $m^{-3}$ or g $dm^{-3}$) |
| $D$ | diffusion coefficient ($m^2\ s^{-1}$) |
| $E_b$ | ohmic potential drop across bulk solution (V) |
| $E_{bl}$ | ohmic potential drop across boundary layer (V) |
| $E_D$ | Donnan potential difference (V) |
| $E_{el}$ | difference between the electrode potentials for anode and cathode processes (V) |
| $E_j$ | junction potential difference across boundary layer (V) |
| $E_m$ | ohmic potential drop across membrane (V) |
| $E_{tot}$ | overall stack voltage (V) |
| $F$ | Faraday constant (C equiv.$^{-1}$) |
| [HCl] | hydrochloric acid concentration (mol $m^{-3}$ or g $dm^{-3}$) |
| [HL] | lactic acid concentration (mol $m^{-3}$ or g $dm^{-3}$) |
| $I$ | current (A) |
| $i$ | current density (A $m^{-2}$) |
| $J$ | ion flow rate through the membrane (mol $s^{-1}$) |
| $K$ | mass transfer coefficient (m $s^{-1}$) |
| [$L^-$] | lactate ion concentration (mol $m^{-3}$ or g $dm^{-3}$) |
| $m_{HL}$ | lactic acid amount (g) |
| $m_{NaL}$ | sodium lactate amount (g) |
| $MW$ | molecular weight (g $mol^{-1}$) |
| $N_W$ | water flow rate through the membrane ($m^3\ s^{-1}$) |
| $n_c$ | number of cells |
| [NaCl] | sodium chloride concentration (mol $m^{-3}$ or g $dm^{-3}$) |
| [NaL] | sodium lactate concentration (mol $m^{-3}$ or g $dm^{-3}$) |
| $Q$ | volumetric flow rate ($m^3\ s^{-1}$ or $dm^3\ min^{-1}$) |
| $q$ | outlet flow rate in feed-and-bleed operation mode ($m^3\ s^{-1}$ or $dm^3\ min^{-1}$) |
| $R$ | production rate (mol $s^{-1}$) |
| $R$ | resistance (Ω) |
| $R$ | universal gas constant (J $mol^{-1}K^{-1}$) |
| $r$ | reflux ratio in feed-and-bleed operation mode, $(Q^0 - q)/Q^0$ |
| $r_b$ | ohmic resistance of bulk solution calculated for unit cross section (Ω $cm^2$) |
| $r_{bl}$ | ohmic resistance of boundary layer calculated for unit cross section (Ω $cm^2$) |
| $r_m$ | ohmic resistance of the membranes calculated for unit cross section (Ω $cm^2$) |
| $T$ | absolute temperature (K) |
| $t$ | time (s or min) |
| $t^+$ | transport number of the cation in solution |
| $t^-$ | transport number of the anion in solution |
| $t_a^+$ | transport number of the cation in the anion-exchange membrane |
| $t_c^+$ | transport number of the cation in the cation-exchange membrane |
| $t_a^-$ | transport number of the anion in the anion-exchange membrane |
| $t_c^-$ | transport number of the anion in the cation-exchange membrane |
| $t_w$ | water transport number in the membranes (mol $F^{-1}$) |
| $u$ | ion mobility ($m^2\ s^{-1}\ V^{-1}$) |
| $V$ | volume ($m^3$ or $dm^3$) |
| $\tilde{V}$ | water molar volume ($m^3\ mol^{-1}$) |
| $Z$ | valence |
| $z$ | length coordinate along a direction perpendicular to the membranes (m) |

*Subscripts*

| | |
|---|---|
| a | anion-selective membrane |
| aq | aqueous |
| c | cation-selective membrane |
| comp | compartment |
| d | diffusive |

*Author to whom all correspondence should be addressed.

0021-891X  

exp experimental
fin final
in initial
*k* generic compartment or reservoir
*l* generic cell
m membrane
o osmotic
r entering the reservoir in feed-and-bleed operation mode
tank reservoir
th theoretical
w water

*Superscripts*

± either cation or anion
o entering the cell
wa wall, anion-selective membrane
wc wall, cation-selective membrane

*Greek letters*

$\gamma$ rate of sodium lactate recovery (g $s^{-1}$ or g $min^{-1}$)
$\Gamma$ sodium lactate recovery (%)
$\Delta$ variation, absolute value
$\Delta$mol variation of mols, absolute value (mol)
$\delta$ boundary layer thickness (m)
$\Theta$ current efficiency (%)
$\Lambda$ equivalent conductivity (S $m^2$ equiv.$^{-1}$)
$\rho$ resistivity ($\Omega$m)
$\Psi$ average power requirement (W)
$\Omega$ specific energy requirement (kJ $g^{-1}$)

## 1. Introduction

The first part of this work [1] dealt with the experimental characterization of a single-step isolation and purification process of lactic acid from sodium lactate solutions through electrodialysis. However, the design and optimization of an industrial process can be more easily carried out by using a mathematical model to reproduce its main features [2, 3]. The main purpose of this work has been to set up a mathematical model able to reproduce the behaviour of an electrodialysis unit for recovering lactic acid from sodium lactate solutions. Moreover, since some model parameters depend on the particular process considered and cannot be deduced from the literature, we have also developed a reliable procedure for estimating such parameters based on a few experimental data. Finally, an example of application of the model is reported.

## 2. Mathematical model

This work takes into account the isolation of free lactic acid from sodium lactate solutions by a double decomposition reaction using a four-compartment electrodialyser (see Fig. 1 in [1]). Cation and anion-exchange membranes are arranged in alternate pattern for defining each compartment. Spacer screens, placed between the membranes, usually provide a sheet flow of the solutions in each compartment.

Several tests were performed using this cell configuration and operating in a batch recirculation operation mode (see Fig. 1), and were thoroughly discussed elsewhere [1]. The primary purpose of this work is to develop a model able to reproduce the experimental findings.

To illustrate the behaviour of an electrodialysis stack, we consider the simple model shown in Fig. 2. When a salt solution is pumped through the cell under the influence of an electric field, the cations migrate toward the cathode and the anions toward the anode. The cations pass through the cation-exchange membranes but they are retained by the anion-exchange ones. The opposite is true for the anions. The overall result is an increase in the electrolyte concentrations in two compartments, and a corresponding decrease in the other two.

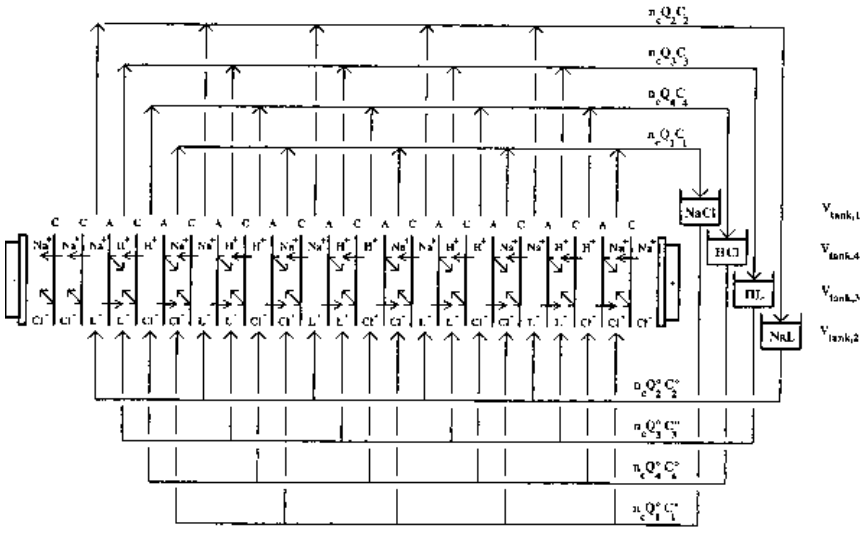


Fig. 1. Sketch of the batch recirculation operation mode of a four-compartment electrodialysis stack for recovering lactic acid (HL) from sodium lactate (NaL) solutions.

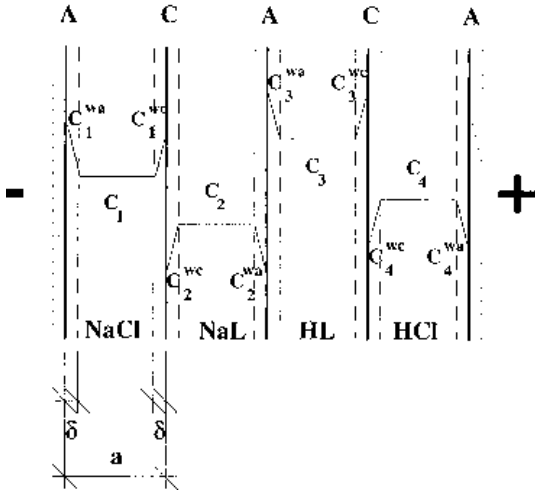


Fig. 2. Cell model. A and C indicate anion and cation-selective membranes, respectively, while $C_k$ are the concentrations.

The ion flux through the membranes can be represented as the sum of two terms: the former due to the applied electric field, and the latter to ion diffusion [2, 3]

$$J_{\mathrm{m}}^{\pm} = \frac{t_{\mathrm{m}}^{\pm} iA}{F} + J_{\mathrm{d}}^{\pm} \tag{1}$$

Similarly, water transport through the membranes from the feed streams to the product streams can occur. This phenomenon is due both to the migration of water molecules associated with ions (this is proportional to the current density and is called electroosmosis), and to osmosis caused by the difference in concentration across the membrane [3]

$$N_{\mathrm{w}} = \frac{t_{\mathrm{w}} \tilde{V} iA}{F} + J_{\mathrm{wo}} \tag{2}$$

Usually, both ion diffusion and osmotic water transfer are negligible with respect to the other fluxes. In particular, dedicated tests have shown that this is true for the commercial membranes used in the tests to be reproduced [1]. As a consequence, ion and water transport through the membranes can be approximated by the following expressions:

$$J_{\mathrm{m}}^{\pm} \cong \frac{t_{\mathrm{m}}^{\pm} iA}{F} \tag{3}$$

$$N_{\mathrm{w}} \cong \frac{t_{\mathrm{w}} \tilde{V} iA}{F} \tag{4}$$

Simulation of the batch recirculation operation mode requires a dynamic mathematical model. Assuming uniform concentration inside each compartment and reservoir, the mass balance equations reported below represent the variation of concentrations, volumes, and flow rates of the system. The small boundary layers adjacent to the membranes (see Fig. 2) have not been considered in such balances. Moreover, since each compartment and reservoir have been considered as a perfectly mixed region, the internal concentration is equal to that of the outlet stream.

Assuming constant density, the mass balance equations for the solute in each compartment result in

$$V_{\mathrm{comp},k} \frac{\mathrm{d}C_k}{\mathrm{d}t} = Q_k^0 C_k^0 - Q_k C_k + J_k \tag{5}$$

while for the solution

$$Q_k^0 - Q_k + N_{\mathrm{w}k} = 0 \tag{6}$$

$J_k$ and $N_{\mathrm{w}k}$ are, respectively, the net fluxes of ions and water entering each compartment:

$$J_k = \pm\left(t_{\mathrm{c}k}^{+} - t_{\mathrm{a}k}^{+}\right)\frac{iA}{F} = \pm\left(t_{\mathrm{a}k}^{-} - t_{\mathrm{c}k}^{-}\right)\frac{iA}{F} \tag{7}$$

$$N_{\mathrm{w}k} = \pm\frac{t_{\mathrm{w}k}\tilde{V} iA}{F} \tag{8}$$

Both $J_k$ and $N_{\mathrm{w}k}$ are positive for the product compartments, that is, for sodium chloride and lactic acid compartments ($k$ = 1 and 3, see Fig. 2), while they are negative for the feed compartments ($k$ = 2 and 4, see Fig. 2).

While Equations 5 and 7 are straightforward for strong binary electrolytes such as sodium chloride (in this case the solute is completely dissociated and anion and cation concentrations are equal to each other and to the overall solute concentration), a more detailed analysis is needed for weak electrolytes. For the lactic acid compartment the balance equation for undissociated lactic acid is

$$V_{\mathrm{comp},3}\frac{\mathrm{d}[\mathrm{HL}]_3}{\mathrm{d}t} = Q_3^0[\mathrm{HL}]_3^0 - Q_3[\mathrm{HL}]_3 + R^{\mathrm{HL}} \tag{9}$$

In this case the flux through the membrane disappears, while a new term representing the lactic acid production rate due to the equilibrium reaction

$$\mathrm{HL_{aq}} \Longleftrightarrow \mathrm{H_{aq}^{+}} + \mathrm{L_{aq}^{-}} \tag{10}$$

has to be considered. Similarly, the mass balance equation for lactate ions is

$$V_{\mathrm{comp},3}\frac{\mathrm{d}[\mathrm{L}^{-}]_3}{\mathrm{d}t} = Q_3^0[\mathrm{L}^{-}]_3^0 - Q_3[\mathrm{L}^{-}]_3 + J_3 + R^{\mathrm{L}^{-}} \tag{11}$$

Since lactic acid is a monovalent acid, $R^{\mathrm{L}^{-}} = -R^{\mathrm{HL}}$. Thus, the variation of the overall concentration of lactic acid (both dissociated and nondissociated: $C_3 = [\mathrm{HL}]_3 + [\mathrm{L}^{-}]_3$) can be deduced from the sum of Equations 9 and 11, leading to

$$V_{\mathrm{comp},3}\frac{\mathrm{d}C_3}{\mathrm{d}t} = Q_3^0 C_3^0 - Q_3 C_3 + J_3 \tag{12}$$

which is the same as Equation 5. Similarly, mass balance equations for the solute and the solution in the reservoirs are

$$\frac{\mathrm{d}\left(C_k^0 V_{\mathrm{tank},k}\right)}{\mathrm{d}t} = n_{\mathrm{c}}\left(Q_k C_k - Q_k^0 C_k^0\right) \tag{13}$$

$$\frac{\mathrm{d}\left(V_{\mathrm{tank},k}\right)}{\mathrm{d}t} = n_c\left(Q_k - Q_k^0\right) = n_c N_{\mathrm{w}k} \tag{14}$$

Equations 5 to 8, 13 and 14 lead to a system of 16 equations in the 16 unknowns $C_k$, $C_k^0$, $Q_k$, and $V_{\mathrm{tank},k}$ ($k$ = 1 to 4), that can be solved only if the current density is known. However, in this case the evaluation of the overall stack voltage is also required to compute the process efficiency.

The overall potential drop across an electrodialysis stack consists of the ohmic potential drops ($IR$), the Donnan potential differences ($E_D$), the junction potential differences ($E_j$), and the electrode potential difference ($E_{el}$), according to the expression [4, 5]:

$$E_{tot} = n_c\left(IR + E_D + E_j\right) + E_{el} \tag{15}$$

The ohmic potential drops vanish rapidly when interrupting the current, whereas the potential differences $E_D$ and $E_j$ relax more slowly because their relaxation depends on ionic diffusion. Spiegler [5] showed that the overall stack voltage can be computed as the sum of two terms: one is linear in $i$ and the other is a logarithmic function of $i$. Ohmic potential drops in the boundary layers adjacent to the membranes are contained in the second term together with the Donnan and junction potential differences.

All the potential drop expressions can be written considering the simple model represented in Fig. 2. Electric potential gradients have been taken as the potential on the right side minus the potential on the left one (divided by the distance); therefore, in Fig. 2, the electric potential gradient is positive.

The ohmic potential drops are established in the bulk of the solutions, in the boundary layers adjacent to the membranes and in the membranes:

$$IR = E_b + E_{bl} + E_m \tag{16}$$

The overall ohmic potential drop in the membranes for a single cell is

$$E_m = r_m i \tag{17}$$

Note that since the model does not distinguish between the ohmic resistance of the cation and anion-exchange membranes, an effective value, equal to the sum of the ohmic resistances (for unit cross section) of all the membranes in a cell, has been considered.

The ohmic resistance (again for unit cross section) of bulk solution can be expressed by

$$r_{bk} = \rho(a - 2\delta) \simeq \frac{a}{C_k \Lambda_k} \tag{18}$$

The ohmic potential drop in each cell is

$$E_b = \sum_{k=1}^{4} \frac{a}{C_k\,\Lambda_k} i \tag{19}$$

For calculating the ohmic resistance (again for unit cross section) of a boundary layer it is necessary to integrate the specific resistance of the solution over the boundary layer thickness:

$$r_{bl} = \int_0^{\delta} \rho \mathrm{d}z = \int_0^{\delta} \frac{1}{C\,\Lambda} \mathrm{d}z \tag{20}$$

Equation 20 can be integrated assuming a linear concentration gradient in the boundary layer [5] (see also Equations 26 to 29 below):

$$\frac{\mathrm{d}C_k}{\mathrm{d}z} = \frac{\left(t_{ak}^- - t_k^-\right) i}{D_k F} = \frac{\left(t_{ck}^+ - t_k^+\right) i}{D_k F} \tag{21}$$

Substituting Equations 21 in Equation 20, the ohmic potential drop across the boundary layer results, for an ideally selective anionic membrane ($t_{ak}^- = 1$) in

$$E_{bl,ak} = \pm \frac{B_k}{t_k^+} \ln\left(\frac{C_k}{C_k^{wa}}\right) \tag{22}$$

and for an ideally selective cationic membrane ($t_{ck}^+ = 1$)

$$E_{bl,ck} = \pm \frac{B_k}{t_{-k}} \ln\left(\frac{C_k}{C_k^{wc}}\right) \tag{23}$$

where $B_k$ is defined (with $D$ and $\Lambda$ taken constant with $C$) as

$$B_k = \frac{D_k F}{\Lambda_k} \tag{24}$$

and the signs + and − refer to the feed ($k$ = 2 and 4) and product ($k$ = 1 and 3) compartments, respectively.

The overall ohmic potential drop in the boundary layers is

$$E_{bl} = \sum_{k=1}^{4} \left(E_{bl,ak} + E_{bl,ck}\right) \tag{25}$$

Wall concentrations can be computed assuming steady-state for the boundary layers [2, 3, 5]. In this case, the combined electrical and diffusive flux through the boundary layer equals the flux through the membrane:

$$\frac{t_{ak}^- iA}{F} = \frac{t_k^- iA}{F} \pm K\left(C_k^{wa} - C_k\right)A \tag{26}$$

$$\frac{t_{ck}^+ iA}{F} = \frac{t_k^+ iA}{F} \pm K\left(C_k^{wc} - C_k\right)A \tag{27}$$

where the signs + and − refer to the product ($k$ = 1 and 3) and feed ($k$ = 2 and 4) compartments, respectively. Wall concentration values can be deduced from the equations above:

$$C_k^{wa} = C_k \pm \frac{i}{FK}\left(t_{ak}^- - t_k^-\right) \tag{28}$$

$$C_k^{wc} = C_k \pm \frac{i}{FK}\left(t_{ck}^+ - t_k^+\right) \tag{29}$$

Although the mass transfer coefficient is different for each compartment, an average effective value has been used. This simplification is justified by the values of the diffusion coefficients being quite close to one another, and by the same fluid dynamic conditions prevailing in each compartment.

The electric potential difference across an ion-selective membrane in contact with two electrolyte solutions is referred to as the Donnan potential difference, and can be described by the following expression [5, 6]:

$$E_{Dk/k+1} = \pm \frac{RT}{F} \ln\left(\frac{C_{k+1}^w}{C_k^w}\right) \tag{30}$$

where $k/(k+1)$ indicates the membrane between compartments $k$ and $k+1$, and the signs + and − refer to anion or cation-selective membranes, respectively. The overall Donnan potential difference for a cell is given by

$$E_D = \frac{RT}{F}\ln\left(\frac{C_1^{wa}}{C_4^{wa}}\frac{C_1^{wc}}{C_2^{wc}}\frac{C_3^{wa}}{C_2^{wa}}\frac{C_3^{wc}}{C_4^{wc}}\right) \quad (31)$$

Finally, the overall junction potential difference in the boundary layers for a cell can be written as [5, 6]

$$E_j = \frac{RT}{F}\sum_{k=1}^{4} \pm\left(t_k^- - t_k^+\right)\ln\frac{C_k^{wc}}{C_k^{wa}} \quad (32)$$

where the signs + and − refer to the product ($k$ = 1 and 3) and feed ($k$ = 2 and 4) compartments, respectively.

Again, both Donnan and junction potential differences are considered positive when the right side is more positive than the left (see Fig. 2).

Equations 15 to 32 provide a correlation between current density and overall stack voltage, thus completing the mathematical model.

## 3. Parameter estimation

Several parameters involved in the model are summarized in Table 1. Apart from the geometrical characteristics of the system, a few parameters can be taken from the literature.

Ion transport numbers in solution have been computed using the expression

$$t_k^{\pm} = \frac{u_k^{\pm} Z_k C_k}{\Sigma_k\left(u_k^{\pm} Z_k C_k\right)} \quad (33)$$

The ionic mobility values have been deduced from those of the equivalent conductivity, which in turn have been either obtained from the literature [7], or determined based on experimental measurements [8].

Diffusion coefficients have been estimated following the procedure reported in [9]. However, a few parameters can be neither deduced from the literature, nor estimated on the basis of suitable relationships. They can be tuned using experimental data from an electrodialysis stack working in a batch recirculation operation mode. The estimation procedure, which makes use of a set of tests reported elsewhere [1], is illustrated in the following, while the main operating conditions involved in the tests are summarized in Table 2.

*Table 2. Ranges of the main operating conditions for experimental runs 1 to 8 reported in [1]*

| | |
|---|---|
| Operation mode | Batch recirculation |
| [NaCl] / g dm$^{-3}$ | 22–49 |
| [NaL] / g dm$^{-3}$ | 1–127 |
| [HL] / g dm$^{-3}$ | 47–412 |
| [HCl] / g dm$^{-3}$ | 1–10 |
| $i$ / A m$^{-2}$ | 110–300 |
| Run time / min | 0–150 |
| Temperature / °C | 21 |
| Flow rate/ dm$^3$ min$^{-1}$ | 0.3 (entering each compartment) |
| Number of cells | 5 |
| Voltage / V | 0–35 |
| Anion-selective membrane | Neosepta AMX, Tokuyama Soda |
| Cation-selective membrane | Neosepta CMX, Tokuyama Soda |

The ion transport number in the membrane is strictly related to the experimental conditions (see Table 2), and determines the membrane selectivity. From Equations 5, 7 and 13 the overall transport of solute is given by (for $V_{comp,k}\ C_k \ll V_{tank,k}\ C_k^0$)

$$\frac{d(V_{tank,k}\ C_k^0 + n_c(V_{comp,k}\ C_k))}{dt} \cong \frac{d(V_{tank,k}\ C_k^0)}{dt} = n_c J_k = \pm(t_{ck}^+ - t_{ak}^+)\frac{iA}{F}n_c = \pm(t_{ak}^- - t_{ck}^-)\frac{iA}{F}n_c \quad (34)$$

*Table 1. Model parameter values*

| *Parameter* | *Value* | *Reference* |
|---|---|---|
| $n_c$ | 5 | [1] |
| $A$ / m$^2$ | 0.02 | [1] |
| $a$ / mm | 0.75 | [1] |
| $V_{comp,\,k}$ / m$^3$ | $0.015 \times 10^{-3}$ | [1] |
| $u_k^{\pm}$ / m$^2$ s$^{-1}$ V$^{-1}$ | $u_{Na^+} = 5.2 \times 10^{-8}$; $u_{L^-} = 4.5 \times 10^{-8}$<br>$u_{H^+} = 36.3 \times 10^{-8}$; $u_{Cl^-} = 7.9 \times 10^{-8}$ | [7,8] |
| $t_k^{\pm}$ | $t_{NaL}^+ = 0.54$; $t_{NaL}^- = 0.46$<br>$t_{HL}^+ = 0.89$; $t_{HL}^- = 0.11$<br>$t_{HCl}^+ = 0.82$; $t_{HCl}^- = 0.18$<br>$t_{NaCl}^+ = 0.40$; $t_{NaCl}^- = 0.60$ | [7,8] |
| $D_k$ / m$^2$ s$^{-1}$ | $D_{NaL} = 1.2 \times 10^{-9}$; $D_{HCl} = 3.3 \times 10^{-9}$<br>$D_{HL} = 2.1 \times 10^{-9}$; $D_{NaCl} = 1.6 \times 10^{-9}$ | [9] |
| $t_m^{\pm}$ | $t_c^+ = 1$; $t_a^+ = 0$<br>$t_c^- = 0$; $t_a^- = 1$ | [1] |
| $t_{wk}$ / mol F$^{-1}$ | $t_{wNaL} = 16.3$; $t_{wHCl} = 7.3$<br>$t_{wHL} = 12.6$; $t_{wNaCl} = 11.0$ | [1] |
| $r_m$ / Ω cm$^2$ | 18.9 | this work |
| $K$ / m s$^{-1}$ | $1 \times 10^{-3}$ | this work |
| $E_{el}$ / V | 2.7 | this work |

Assuming constant membrane transport numbers, Equation 34 can be integrated for runs carried out at constant current density to give

$$\Delta(V_{\text{tank},k}\, C_k^0) = \Delta\text{mol}_k = (t_{ck}^+ - t_{ak}^+)\frac{iA}{F} t\, n_c \qquad (35)$$

This relates the experimental variation of mols in each reservoir ($\Delta\text{mol}_k$) to the theoretical mols ($iAtn_c/F$) through the transport number values in the membranes.

Representing all the experimental results in terms of experimental mols transported during the process versus the theoretical mols, it is noted that the corresponding values are almost equal (see Fig. 8 in [1]). This means ideal behaviour of the membranes, that is, the values of transport numbers in the membranes are equal to one or zero, as shown in Table 1. It should be noted that this condition of ideality also arises from the negligible permeation of both water and ions with respect to electro-transport, as previously mentioned.

The equations describing water flux through the membranes (Equations 8 and 14) show that reservoir volumes depend on the transport number of water for each solution. From such equations, the volume variation of each tank can be easily computed for constant current density values:

$$\Delta V_{\text{tank},k} = \frac{n_c\, t_{wk} \tilde{V} iAt}{F} \qquad (36)$$

Again, volume variation values are related to the electric charge through the water transport numbers. The values of $t_{wk}$ have been calculated by linear regression on the volume variations for all the reservoirs (see Fig. 7 in [1]). It can easily be seen from Equation 36 that the water transport numbers must fulfil the constraint

$$(t_{\text{wNaCl}} + t_{\text{wHL}}) - (t_{\text{wNaL}} + t_{\text{wHCL}}) = 0 \qquad (37)$$

The estimated values fulfil this constraint with a percentage error of less than 10%: this is good evidence of the reliability of the proposed approach. However, the values obtained have been reconciled to obtain the values reported in Table 1.

The last three unknown parameters listed in Table 1 (i.e., the ohmic resistance of the membranes, the mass transfer coefficient from the bulk solution to the membrane, and the difference between the electrode potentials for anode and cathode processes) are related to the overall stack voltage. The typical experimental profile of the stack voltage versus time for a batch recirculation operation mode is shown in Fig. 3b. For the largest part of the run time the stack voltage is almost constant, while in the last few minutes it increases sharply. This is due to the concentration value in one of the feed compartments approaching zero. The proposed model is able to represent such a qualitative behaviour well, regardless of the parameter values. To also obtain quantitative agreement they have been tuned on the initial stack voltage values (in order to reproduce the largest part of the curve), as well as on the final run time values, using half the runs reported in [1]. This last estimating procedure requires a non-linear multiparameter optimization routine. The average percentage error between the experimental data used for the estimating procedure and the calculated values is about 16%. Since only one half of the available experimental data have been used for the tuning procedure, a comparison can be made between this average percentage error and that computed considering the runs not used for estimating the adjustable parameters (in this case the model is predictive). The obtained value (equal to 7%) is close to that obtained previously, thus confirming the reliability of the estimated values of the adjustable parameters.

## 4. Comparison with experimental data

A typical comparison between experimental [1] and computed values is shown in Fig. 3, where the variations in both the reservoir concentrations and the stack voltage against time are reported. Since these data were not used in the fitting procedure for $r_m$, $K$ and $E_{el}$, in this case the model is predictive. The good agreement between experimental data and model simulations confirms the reliability of the model predictions. In particular, it is possible to observe a reasonable agreement with the experimental results concerning the stack voltage in the final part of the curve in spite of the considerable reductive assumptions of the model. However, a more useful comparison can be carried out considering some overall process performance indices: specific energy ($\Omega$) and power ($\Psi$) requirements, defined in Table 3, and sodium lactate recovery ($\Gamma$) and current efficiency ($\Theta$), defined as follows:

$$\Gamma = \frac{(m_{\text{NaL,in}} - m_{\text{NaL,fin}})}{m_{\text{NaL,in}}} \times 100 \qquad (38)$$

$$\Theta = \frac{\Delta\text{mol}_{\text{exp}}}{\Delta\text{mol}_{\text{th}}} = \frac{\left(\frac{m_{\text{HL,fin}} - m_{\text{Hl,in}}}{MW}\right)}{(In_c\, t_{\text{fin}})/F} \times 100 \qquad (39)$$

The comparison between experimental [1] and calculated values is shown in Figs 4 and 5. The model predictions are good and are often inside the range of experimental uncertainties. Also in the case of the greatest disagreement ($\Gamma$ for run 6, see [1]), the model is able to correctly predict the experimental trend: this is of paramount importance for optimization studies, as discussed in the following section.

## 5. Parametric analysis

Since all the model parameters estimated on the basis of batch tests depend only on the stack configuration (that is, type of membranes and their arrangement inside the cell) and on the nature of the feed solutions, they can also be used for simulating different process operation modes, such as continuous or feed-and-bleed. However, the mathematical model discussed in

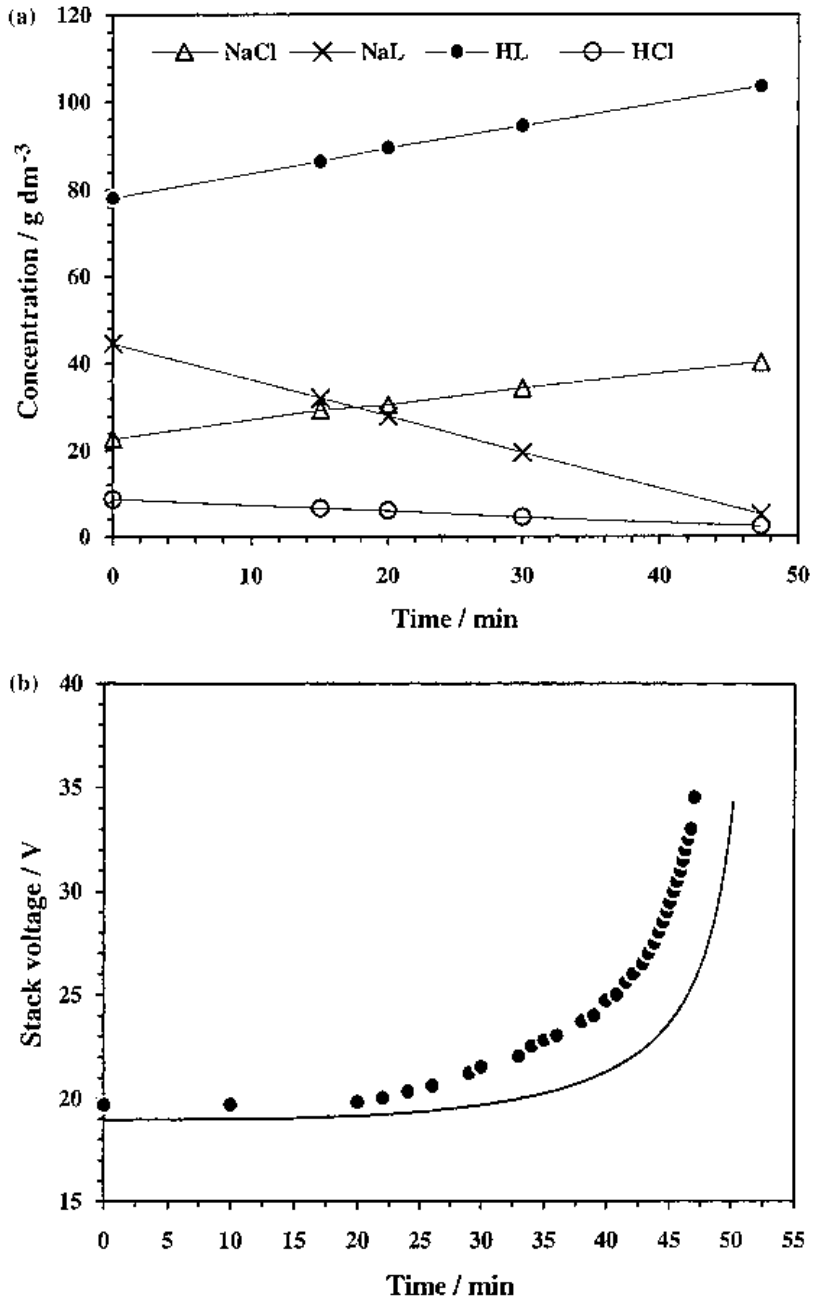


Fig. 3. Comparison between experimental (symbols) and model (lines) results. Experimental data from [1], run 4. (a) Variation of tank concentrations with time. (b) Variation of overall stack voltage with time.

*Table 3. Expression of some overall performance indices for various process operation modes*

| *Process performance index* | *Process operation mode* | | |
|---|---|---|---|
| | *Batch recirculation* (*see Fig. 1*) | *Continuous* (*see Fig. 6*) | *Feed-and-bleed* (*see Fig. 7*) |
| Rate of lactate recovery ($\gamma$) | $\frac{\left(m_{\mathrm{NaL,in}} - m_{\mathrm{NaL,fin}}\right)}{t_{\mathrm{fin}}}$ | $Q^0_{2,1}C^0_{2,1} - Q_{2,\mathrm{n}}C_{2,\mathrm{n}}$ | $Q_{\mathrm{r2}}C_{\mathrm{r2}} - qC_2$ |
| Specific energy requirement ($\Omega$) | $\frac{\int_0^{t_{\mathrm{fin}}}\left(IE_{\mathrm{tot}}\right)\mathrm{d}t}{m_{\mathrm{HL,fin}} - m_{\mathrm{HL,in}}}$ | $\frac{\Psi}{\gamma}$ | $\frac{\Psi}{\gamma}$ |
| Power requirement ($\Psi$) | $\frac{\int_0^{t_{\mathrm{fin}}}\left(IE_{\mathrm{tot}}\right)\mathrm{d}t}{t_{\mathrm{fin}}}$ | $IE_{\mathrm{tot}}$ | $IE_{\mathrm{tot}}$ |

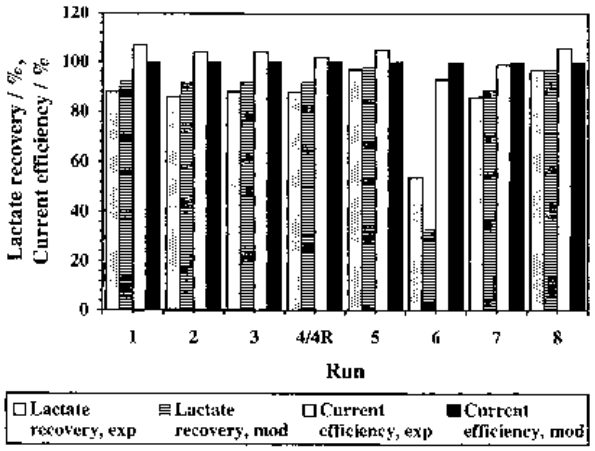


Fig. 4. Comparison between experimental and computed values of sodium lactate recovery and current efficiency . Experimental data from [1], runs 1 to 8. See Table 3 in [1] for run directory.

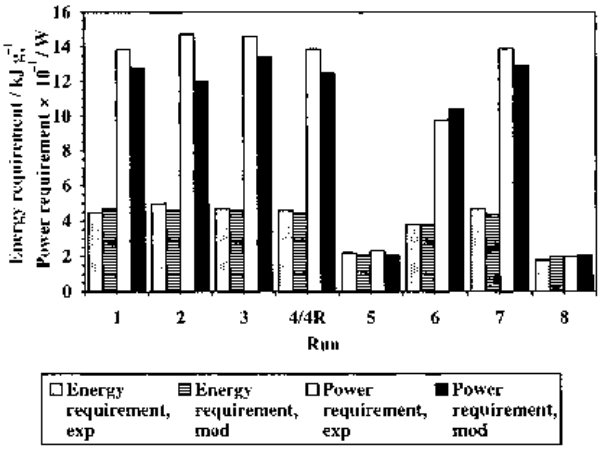


Fig. 5. Comparison between experimental and computed values of specific energy and power requirements. Experimental data from [1], runs 1 to 8. See Table 3 in [1] for run directory.

the previous section has to be modified for representing such process operation modes.

As an example of application of this procedure, the influence of several process operation modes and operating parameters on some overall performance indices is discussed. In particular, three different process operation modes are considered, namely: (i) batch recirculation operation mode, reported in Fig. 1. This is the same used in the experimental tests reported in [1]; (ii) continuous operation mode, shown in Fig. 6. This requires an increase in the number of cells per stack; (iii) feed-and-bleed operation mode, represented in Fig. 7. This should summarize the advantages of the previous operation modes [10, 11]. Only steady state has been considered for the two last operation modes.

Although the $E_{tot}/i$ relationship does not change from batch recirculation to other operation modes, the mass balance equations have to be changed from the previous ones. In particular, for the continuous operation mode Equations 5 and 6 are replaced by

$$Q^0_{k,l}\, C^0_{k,l} + J_k = Q_{k,l}\, C_{k,l} \qquad l = 1 \ldots n \qquad (40)$$

$$Q^0_{k,l} + N_{wk} = Q_{k,l} \qquad l = 1 \ldots n \qquad (41)$$

with the constraints

$$Q_{k,l} = Q^0_{k,l+1} \qquad l = 1 \ldots n-1 \qquad (42)$$

$$C_{k,l} = C^0_{k,l+1} \qquad l = 1 \ldots n-1 \qquad (43)$$

while the mass balances for the reservoirs disappear.

Similarly, the feed-and-bleed operation mode can be represented by the following equations, replacing Equations 5, 6, 13 and 14, respectively

$$Q^0\, C^0_k + J_k\, n_c = Q_k\, C_k \qquad (44)$$

$$Q^0 + N_{wk}\, n_c = Q_k \qquad (45)$$

$$Q_{rk}\, C_{rk} + (Q_k - q)\, C_k = Q^0\, C^0_k \qquad (46)$$

$$Q_{rk} + (Q_k - q) = Q^0 \qquad (47)$$

Equations 44 to 47 lead to a system of 16 equations in the 16 unknowns $C_k$, $C^0_k$, $Q_k$ and $Q_{rk}$ ($k$ = 1 to 4).

For the sake of the example, all process operation modes have been compared in terms of the following overall indices: rate of recovery of sodium lactate ($\gamma$); specific energy requirement ($\Omega$); and power requirement ($\Psi$). These indices have been computed using the expressions reported in Table 3.

Starting from a basis condition, we have investigated the effect of changing several operating parameters, as summarized in Table 4. The results of this analysis are shown in Figs 8 to 10.

Considering the batch recirculation operation mode, it is evident that the optimal condition should be a compromise among different trends. For instance, increasing current density results in an increase in both specific energy and power requirement, while increasing the number of cells increases the rate of lactate recovery and power requirement, but decreases the specific energy requirement. Moreover, an interesting effect is shown by runs 8, 9 and 10 in comparison with the run 'basis' (see Table 4). In these runs the current density, initially equal to that of the run 'basis', is lowered stepwise after a given time: it can be seen that, while the rate of lactate recovery does not decrease very much, the power requirement diminishes markedly. However, total run time increases. There are no large differences between different operation modes apart from the large power requirement of the continuous operation mode, due to the large number of cells required to recover a significant amount of sodium lactate. For the feed-and-bleed operation mode, two different reflux ratios ($r = (Q^0 - q) / Q^0$) values have been considered (runs 11 and 12, see Table 4). From Figs 8 to 10 it appears that the reflux ratio has no influence on the process performance. This is a misleading conclusion, since it refers only to the three indices considered; in this case the $r$ value strongly affects other indices, for instance the recovery of sodium lactate. This is clearly shown in Fig. 11, where the concentration of sodium lactate in the waste stream is shown as a function of $r$. Increasing the reflux ratio, results in a large decrease in

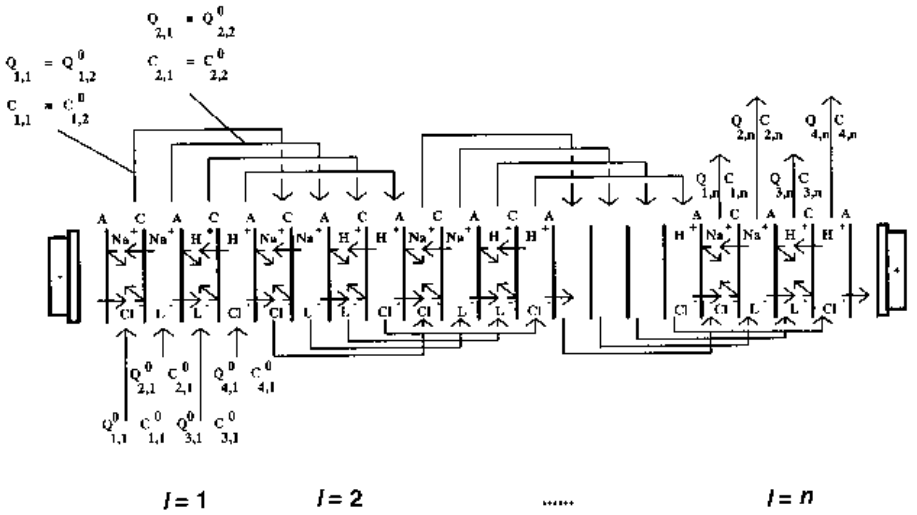


Fig. 6. Sketch of the continuous operation mode for a four-compartment electrodialysis stack.

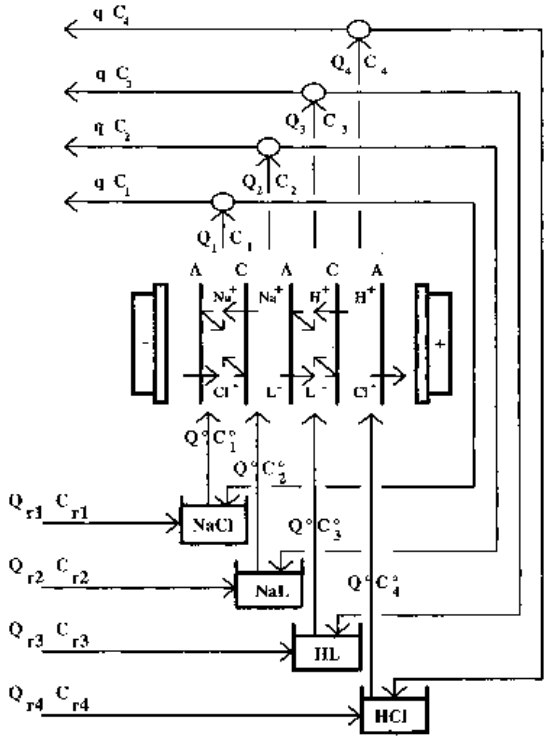


Fig. 7. Sketch of the feed-and-bleed operation mode for a four-compartment electrodialysis stack.

such concentration and, thus, in a larger recovery of sodium lactate.

## 6. Conclusions

In this work a general procedure for developing a simulation model of an operating electrodialysis stack has been presented. It basically consists of the following steps:

(i) The importance of water and solute permeation with respect to electrotransport should be checked. This can be easily done by circulating, in batch recirculation operation mode, concentrated solutions and distilled water in alternate compartments without an electric field, and recording reservoir volume and solute concentration values. Usually, these phenomena do not play a significant role, and this is the case covered by this work. If the opposite is true, the experimental results can be used to model solute ($J_d$) and water ($J_{wo}$) fluxes.

(ii) A few tests in batch recirculation operation mode at constant current density should be performed. This allows estimation of the ion transport numbers and the water transport numbers in the membranes using Equations 35 and 36.

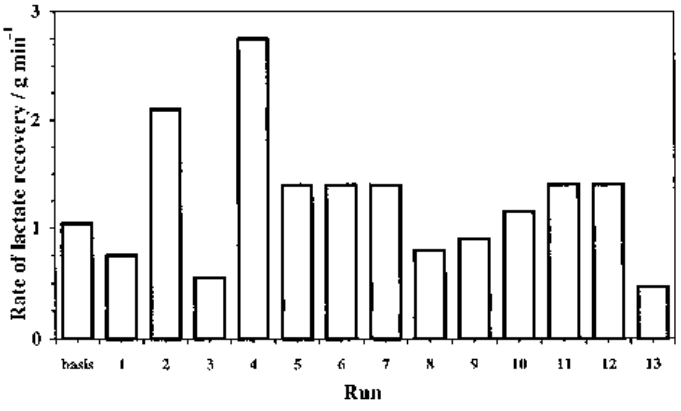


Fig. 8. Parametric analysis results for the rate of sodium lactate recovery. See Table 4 for run directory.

*Table 4. Directory of runs performed for parametric analysis*[*]

| *Run* | *Process operation mode* | *Current density* /A $m^{-2}$ | *Duration time* / min | *Cell number* | *Current–time relationship* |
|---|---|---|---|---|---|
| Basis | batch recirculation | 200 | until $E_{tot}$ = 35 V | 5 | constant |
| 1 | batch recirculation | 100 | until $E_{tot}$ = 35 V | 5 | constant |
| 2 | batch recirculation | 300 | until $E_{tot}$ = 35 V | 5 | constant |
| 3 | batch recirculation | 200 | until $E_{tot}$ = 35 V | 2 | constant |
| 4 | batch recirculation | 200 | until $E_{tot}$ = 35 V | 10 | constant |
| 5 | batch recirculation | 200 | 20 | 5 | constant |
| 6 | batch recirculation | 200 | 30 | 5 | constant |
| 7 | batch recirculation | 200 | 40 | 5 | constant |
| 8 | batch recirculation | 200/100 | until $E_{tot}$ = 35 V | 5 | step variation at $t$ = 20 min |
| 9 | batch recirculation | 200/100 | until $E_{tot}$ = 35 V | 5 | step variation at $t$ = 30 min |
| 10 | batch recirculation | 200/100 | until $E_{tot}$ = 35 V | 5 | step variation at $t$ = 50 min |
| 11 | feed-and-bleed ($r$ = 0.9) | 200 | | 5 | constant |
| 12 | feed-and-bleed ($r$ = 0.1) | 200 | | 5 | constant |
| 13 | continuous | 200 | | 250 | constant |

[*] Other conditions: feed concentration values: [NaCl] = 25 g $dm^{-3}$; [NaL] = 36 g $dm^{-3}$; [HL] = 85 g $dm^{-3}$; [HCl] = 9 g $dm^{-3}$ (apart from run 13: [HCl] = 10 g $dm^{-3}$).

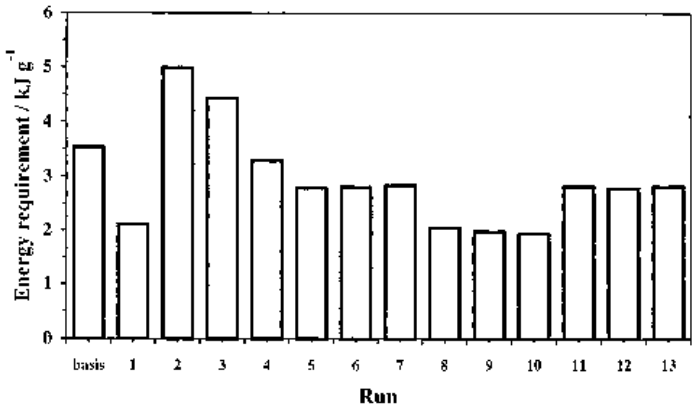


Fig. 9. Parametric analysis results for specific energy requirement. See Table 4 for run directory.

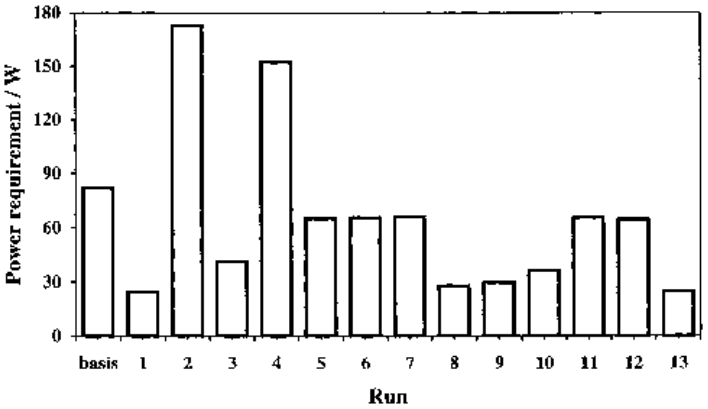


Fig. 10. Parametric analysis results for power requirement. See Table 4 for run directory. Value for run 13 multiplied by $10^{-2}$.

(iii) The three parameters involved in the stack voltage model (i.e., the ohmic resistance of the membranes, the mass transfer coefficient from the bulk solution to the membrane, and the difference between the electrode potentials for anode and cathode processes) can be tuned on the same experimental data.

Using these parameter values, different process operation modes, as well as the influence of several operating parameters, can be investigated leading to

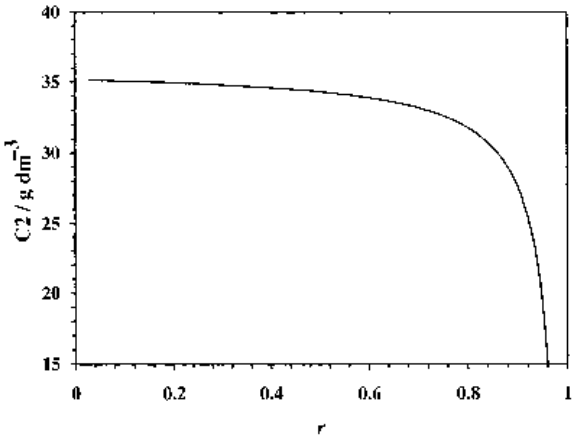


Fig. 11. Concentration of sodium lactate in the waste stream for feed-and-bleed operation mode computed as a function of reflux ratio. See Table 4 for run directory.

the optimization of the process. However, the optimization procedure requires *a priori* definition of the objective function, that is what has to be optimized. Almost any objective function can be easily computed using the model discussed above. Such a model can be considered as a part of an overall optimization flowsheeting package [12]. Finally, it is worth noting that different stack configurations or membranes require a retuning of some parameters. However, the tests required to tune the model can be easily performed using any operating stack.

## Acknowledgements

N. Boniardi acknowledges the financial support to PhD thesis of Sespi s.r.l., Milano.

## References

[1] N. Boniardi, R. Rota, G. Nano and B. Mazza, *J. Appl. Electrochem.* **26** (1996) 125.
[2] F. Evangelista, *Desalination* **64** (1987) 353.
[3] D. Barba, F. Evangelista, G. Jonsson and L. Marrelli, *ibid.* **71** (1989) 137.
[4] D. A. Cowan and J. H. Brown, *Ind. Eng. Chem.* **51** (1959) 1445.
[5] K. S. Spiegler, *Desalination* **9** (1971) 367.
[6] K. J. Vetter, 'Electrochemical Kinetics', Academic Press, New York (1967).
[7] G. Bianchi and T. Mussini, 'Fondamenti di Elettrochimica' (in Italian), Masson, Milano (1993).
[8] N. Boniardi, 'Lactic acid recovery by electrodialysis: experimental tests and mathematical model' (in Italian), PhD thesis, Politecnico di Milano (1995).
[9] R. C. Reid, J. M. Praustnitz and T. K. Sherwood, 'The Properties of Gases and Liquids', McGraw-Hill, New York (1977).
[10] R. Rautenbach and R. Albrecht, 'Membrane Processes', John Wiley & Sons, New York (1989).
[11] M. H. Lopez Leiva, *Lebensm. Wiss. Technol.* **21** (1988) 119.
[12] R. D. La Roche, M. A. Stadtherr and R. C. Alkire, *J. Appl. Electrochem.* **24** (1994) 1206.